An International Journal of Optimization and Control: Theories & Applications
ISSN: 2146-0957 eISSN: 2146-5703
Vol.x, No.x, pp.xx-xx (2026)
https://doi.org/10.36922/IJOCTA026140050

RESEARCH ARTICLE

Neural network-based distributed fault estimation for multi-Area interconnected power systems with actuator faults and network constraints

Nezar M. Alyazidi[1,2], Mutaz M. Hamdan[3†*], Ahmed Eltayeb[2†], Mahmoud S. AbouOmar[2†], Gamil Ahmed[2†] and Maged S. Al-Quraishi[2†]

[1]Control and Instrumentation Engineering Department, King Fahd University of Petroleum & Minerals, Dhahran, Saudi Arabia
[2]Interdisciplinary Research Center for Smart Mobility and Logistics, King Fahd University of Petroleum & Minerals, Dhahran, Saudi Arabia
[3]Robotics and AI Engineering Department, Faculty of Engineering, Al-Ahliyya Amman University, Amman, Jordan
nalyazidi@kfupm.edu.sa; m.hamdan@ammanu.edu.jo; ahmedtaha@kfupm.edu.sa; mahmoud.abouomar@kfupm.edu.sa; gamil.ahmed@kfupm.edu.sa; maged.quraishi@kfupm.edu.sa

ARTICLE INFO

Article history:
Received: March 31, 2026
Revised: May 19, 2026
Accepted: May 22, 2026
Available Online: June 9, 2026

Keywords:
Fault estimator
Distributed observer
Networked control systems
State estimator design
Radial basis function neural network
Power system

ABSTRACT

With the growing reliance of multi-area interconnected power systems on communication networks for large-scale data transmission, sensing, and control, network constraints can impair transient performance. This work develops a unified distributed fault-estimation framework based on a radial basis function neural network (RBF-NN) for multi-area interconnected power systems, addressing both communication constraints and actuator faults. We construct an augmented system by integrating the fault dynamics into the system model, and a distributed observer is developed to simultaneously estimate the system states and fault dynamics. The unknown fault effect is approximated by a radial basis function neural network (RBF-NN). A projection-based adaptation law ensures bounded parameter estimation under modeling uncertainties. State and fault estimates are updated using quantized measurements transmitted over networked channels, maintaining accuracy despite time-varying delays and disturbances. Sufficient stability and performance conditions are established by Lyapunov analysis and LMI conditions, guaranteeing exponential stability of the observer error dynamics and prescribed performance bounds under bounded time-varying delays and quantization effects. A three-area case study is presented, and precise state and fault reconstruction are shown for nominal, delayed, faulted, and worst-case scenarios. The proposed scheme is compared with a quantized H_∞ estimator under actuator faults, time-varying delays, and quantization. The peak deviations of $|\Delta\omega|$, $|\Delta P_{tie}|$, and $|\Delta P_{mech}|$ are reduced approximately 33%, 50%, and 27%, respectively, while maintaining bounded system states and neural weights.

(cc) BY

1. Introduction

Contemporary multi-area interconnected power systems increasingly rely on communication networks for large-scale supervision, sensing, and control. While such networked operation enables efficient coordination, it also introduces communication constraints, including time-varying delays, packet dropouts, and quantization, which may affect system signals. Sensor and actuator faults can seriously affect the system's performance

*Corresponding Author
† *These authors contributed equally to this work.*

and may even destabilize the system. Such challenges call for the development of robust estimation and control strategies to enable reliable operation under uncertainty.

Fault-tolerant control (FTC) has been widely investigated to increase the reliability of systems subject to faults. There are two broad categories of FTC strategies: passive and active. Passive FTC designs inherently robust controllers for a given fault scenario, while active FTC uses fault detection and diagnosis (FDD) mechanisms to detect faults in real-time and allow control reconfiguration. Despite significant progress in the design of FTC, accurate fault estimation is still a fundamental requirement for effective fault compensation.[1] However, the fault diagnosis of large-scale systems is extremely complicated due to the interdependence among interconnected subsystems. Consequently, distributed fault detection and estimation methods have received considerable attention. A distributed fault detection scheme for networked systems with time delays is proposed in.[2] Interval observer-based methods have been developed for fault isolation in fuzzy interconnected systems,[3] and adaptive observer designs have been proposed to improve the accuracy of fault estimation in nonlinear interconnected systems satisfying Lipschitz conditions.[4]

Additionally, the separation principles have been exploited to study integrated fault estimation and accommodation frameworks.[5] The unknown input observers for distributed fault estimation of networked systems with disturbances are designed based on augmented-state observer approaches.[6] However, these techniques usually have drawbacks in scalability, robustness, and computational efficiency for high-dimensional interconnected systems with dynamic uncertainties and partial observability.[7]

Multi-area interconnected power systems are described as large-scale systems consisting of several dynamically coupled subsystems. Faults that originate in one subsystem can propagate throughout the network, impacting the overall system performance. This interdependence complicates the diagnosis of faults and highlights the need for distributed estimation schemes. In this setting, the distributed observers have been intensively studied since they enable local estimation with the limited exchange of information among the subsystems, thus increasing scalability and robustness.

Several observer-based and data-driven approaches have been proposed for fault estimation in interconnected and networked systems.[2,4,6,8–10] Observer-based approaches provide systematic frameworks for state and fault reconstruction, while parity-space formulations provide an alternative diagnosis route.[11,12] Data-driven methods, such as neural network-based approaches, further improve the ability to approximate unknown nonlinear effects.[9,10] However, it remains challenging to integrate these approaches in distributed frameworks subject to communication constraints.

Communication constraints such as time-varying delays, packet dropouts, and quantization have a significant effect on the accuracy and performance of system estimation in networked control systems.[2,13] These effects are particularly significant in power systems where fast and accurate information exchange is crucial for frequency control and tie-line power control.[14] At the same time, increased penetration of renewable energy sources brings more uncertainties and disturbances, which result in more challenges for system operations.[15] T herefore, it is important to design estimation schemes that explicitly take into account the shortcomings introduced by network and actuator failures. Thus, it is essential to develop estimation frameworks that explicitly account for both actuator faults and network-induced uncertainties.

Recently, fuzzy and data-driven approaches have been investigated to deal with nonlinearities and uncertainties. For example, Takagi-Sugeno fuzzy observers have been proposed to estimate the state and the fault simultaneously under Lipschitz conditions. Stability results have been obtained via linear matrix inequalities (LMIs).[16] Similarly, an interval type-2 fuzzy systems-based fuzzy framework is proposed for integrated fault diagnosis and fault-tolerant control in nonlinear networked systems.[17] Lyapunov-Krasovskii based designs have also been utilized to study extensions to stochastic multi-delay systems with multi-source faults.[18] Besides, several well-known H_∞-based techniques have been widely applied to fault detection and fault-tolerant control with time delays.[19,20]

Despite these advances, existing approaches remain limited in simultaneously addressing actuator faults and network-induced constraints within distributed estimation frameworks.

Motivated by these challenges, we propose a unified distributed fault-estimation scheme for multi-area interconnected power systems with actuator faults and communication constraints. The proposed approach introduces the fault dynamics into an augmented system model and employs a distributed observer to simultaneously estimate system states and actuator faults, extending the existing observer-based frameworks.[4,6] The unknown nonlinear fault effects are approximated by a radial basis function neural network (RBF-NN) . A projection-based adaptive law ensures bounded

parameter estimation in the presence of uncertainties.[9,10] Moreover, the framework explicitly takes into account quantization and the time-varying delay in the measurement channels.[2,13]

Hence, this paper proposes a unified distributed fault-estimation scheme for multi-area interconnected power systems subject to actuator faults and communication constraints. The proposed approach embeds fault dynamics into an augmented system model and employs a distributed observer to simultaneously estimate system states and actuator faults, thereby extending existing observer-based frameworks.[4,6] A radial basis function neural network (RBF-NN) is incorporated to approximate unknown nonlinear fault effects, while a projection-based adaptive law ensures bounded parameter estimation in the presence of uncertainties.[9,10] Furthermore, the framework explicitly accounts for quantization and time-varying delays in the measurement channels.[2,13]

The main contributions of this work are summarized as follows:

- A unified distributed fault-estimation framework for multi-area interconnected power systems (MAIPS) that jointly addresses actuator faults and network-induced constraints;
- Development of an augmented system model that incorporates fault dynamics and a distributed observer for the simultaneous estimation of system states and actuator faults;
- Integration of a radial basis function neural network (RBF-NN) to approximate unknown nonlinear fault effects, combined with a projection-based adaptive law to ensure bounded parameter estimation under uncertainties;
- A unified estimation architecture that explicitly accounts for communication constraints, including quantization and time-varying delays, as well as bounded disturbances;
- Derivation of sufficient stability and performance conditions based on a Lyapunov-Krasovskii functional, ensuring exponential mean-square stability and a prescribed ℓ_2 disturbance attenuation level, formulated as computationally efficient LMIs for explicit observer gain design.

The remainder of the paper is organized as follows. Section 2 reviews the related literature and identifies the research gaps. Section 3 presents the MAIPS model, the communication constraints, actuator-fault profiles, RBF-NN estimator, and the proposed observer framework. The main theoretical results are developed in Section 4. Section 5 provides an illustrative example. Section 6 concludes the paper.

2. Literature review

Robust estimation and control in the presence of uncertainty have been well studied in networked control systems. In interconnected power systems, H_∞ based methods have provided a fundamental framework for ensuring stability and disturbance attenuation.

The incorporation of computer networks into control systems, alongside increasing performance demands, raises the dependence on inter-component communication and add s significant system complexity. Although these networks enhance efficiency and decrease costs, they are nevertheless plagued by inherent constraints, such as packet loss, transmission delays, and capacity constraints. The aforementioned defects can significantly impair system performance and, in extreme instances, disrupt the entire networked system. As structural complexity increases, the probability of problems, such as actuator failures, sensor degradation, or related components failures increases. As a result, extensive research has concentrated on FTC, which aims to maintain system stability after the incidence of faults. Active FTC frameworks generally integrate fault detection and diagnosis (FDD) techniques that offer real-time information on fault characteristics and severity, facilitating prompt corrective measures.[1,21,22]

Fault diagnosis in nonlinear dynamic systems has been pursued via observer-based schemes,[8,23] parity space formulations,[11,12] and data-driven approaches such as neural networks and fuzzy methods.[9,10] This work focuses on observer-based methods for fault-tolerant control. Discretization and sampling effects are major problems in FTC design, and this is further aggravated by the presence of unobservable system states. These challenges prompt the re-engineering of control structures to handle actuator defects and the design of observers that can accurately reconstruct hidden states. Moreover, the modeling process is often complicated by nonlinear dynamics, making the construction of observers becomes more difficult, especially in systems with highly complex and unpredictable interactions among variables. Some previous studies have addressed similar problems by applying the nonlinear regulation theory to solve the NFTC challenges in applications such as AC motors and robotic manipulators.[24,25] The loss of actuator effectiveness for control-affine nonlinear models was tackled using Lyapunov-based reconstruction approaches.[26] Customized observer

designs have been developed for fault detection, isolation, and compensation in the presence of actuator failures for complex multi-input multi-output (MIMO) nonlinear systems.

Table 1 shows feature comparison of control/estimation for networked power systems.

3. Multi-area interconnected power system model

This study employs a discrete-time representation of an interconnected multi-DC microgrid power system, obtained via linearization around specific operating conditions. The mathematical formulation of the time-invariant power is presented herein. Let N represent the collection of interconnected areas linked via tie-lines. Each subsystem communicates over a networked framework, and the resulting system dynamics can be expressed as follows:

$$\begin{aligned} \mathcal{X}_{ip}(k+1) &= A_{ip}\mathcal{X}_{ip}(k) + B_{ip}\mathcal{U}_{ip}(k) \\ &+ \mathcal{D}_{ip}W_{ip}(k) \\ &+ \psi_{ip}(\mathcal{X}_{ip}, \mathcal{Y}_{ip}, \mathcal{U}_{ip})\theta_{ip}(k) \\ \mathcal{Y}_{ip}(k) &= C_{ip}\mathcal{X}_{ip}(k) \end{aligned} \tag{1}$$

Table 1. Feature comparison of control/estimation for networked power systems

Citation	MA-LFC	Actuator faults	Time-varying delays (S/A)	Log quant.	DO	Stability type	Gap vs. this work
[27]	✗	✗	S: ✓ A: ✗	✗	✗	Exp. MSS/H_∞	Packet dropouts; observer-based H_∞ but not MA-LFC; no faults, no quantization.
[28]	✗	✗	S: ✓ A: ✗	✗	✗	Stochastic	DoS-centric; no distributed observation, no faults, no quantization.
[29]	✗	✗	S: ✓ A: ✗	✗	✗	Stochastic exp.	Deception on measurement only; no faults; no DO; no quantization.
[30]	✗	✗	S: ✓ A: ✗	✗	✓	H_∞	Packet loss/deception treated separately; no actuator faults; no quantization.
[31,32]	✗	✗	S: ✗ A: ✗	✗	3†	Stochastic/H_∞	FDI/FE-focused; not MA-LFC; no joint treatment of faults+quantization.
[33]	✗	✓	S: ✗ A: ✗	✗	✓	Exponential	MAS with DoS + actuator faults via distributed observers; not MA-LFC; no quantization.
[34]	✗	✗	S: ✗ A: ✗	✗	✓	H_∞	DC microgrids with sensor faults and DO; not MA-LFC; no quantization; no actuator faults.
This work	✓	✓	**S: ✓ A: ✓**	✓	✓	**Exp. MSS + ℓ_2-gain**	**Jointly handles faults, S/A delays, and log quantization in MA-LFC via a distributed observer with explicit design recipe.**

Notes: †Mu (2023) is distributed fault *estimation*; Peng (2010) is NCS fault detection (centralized). Both are not MA-LFC.

To clarify this equation, let $\mathcal{X}_{ip}(k) = [\Delta\omega, \Delta P_{mech}, \Delta P_{vi}, \Delta P_{tie,i}]^T \in \Re^n$ denote the state vector, comprising frequency, mechanical power, steam valve position variations, and the variation of the total tie-line power flow. The control input is $\mathcal{U}_{ip} \in \Re^m$. $\mathcal{Y}_{ip} = [\Delta\omega_i,\ \Delta P_{\text{tie},i}]^T \in \Re^p$ indicates the measured output of each subsystem, consisting of deviations in the local frequency and the net tie-line power flow. The signal $W_{ip}(k)$ characterizes the local zero-mean load variation. For a detailed account, see.[14] The system matrices are specified as follows:

$$A_{ip} = \begin{bmatrix} -\frac{D_i}{M_i^a} & \frac{1}{M_i^a} & 0 & -\frac{1}{M_i^a} \\ 0 & -\frac{1}{T_{CH_i}} & \frac{1}{T_{CH_i}} & \\ -\frac{1}{R_i^f T_{gi}} & 0 & -\frac{1}{T_{gi}} & 0 \\ \sum_{j\in\mathcal{J}_n} T_{ij} & 0 & 0 & 0 \end{bmatrix}$$

$$B_{ip} = \begin{bmatrix} 0 \\ 0 \\ 0 \\ \frac{1}{T_{\mathcal{G}_i}} \end{bmatrix}, D_{ip} = \begin{bmatrix} -\frac{1}{M_i^a} \\ 0 \\ 0 \\ 0 \end{bmatrix}$$

$$C_{ip} = \begin{bmatrix} 1 & 0 & 0 & 0 \\ 0 & 0 & 0 & 1 \end{bmatrix}$$

The aggregated representation of the overall interconnected system captures the essential dynamics of each local area i and is expressed as

$$A_i = \text{diag}\Big(A_{1p}, A_{2p}, A_{3p}, \ldots, A_{Np}\Big),$$

$$B_i = \text{diag}\Big(B_{1p}, B_{2p}, B_{3p}, \ldots, B_{Np}\Big),$$

$$C_i = \text{diag}\Big(C_{1p}, C_{2p}, C_{3p}, \ldots, C_{Np}\Big),$$

$$D_i = \text{diag}\Big(D_{1p}, D_{2p}, D_{3p}, \ldots, D_{Np}\Big),$$

$$\psi_i = \text{diag}\Big(\psi_{1p}, \psi_{2p}, \psi_{3p}, \ldots, \psi_{Np}\Big)$$

Table 2 summarizes the generation area parameters of the multi-area interconnected power system, where different regions are characterized by their generator specifications. Key parameters include mechanical output power, inter-area power flow, rotor angular frequency, governor response time, and load variation. These variables play a crucial role in ensuring operational reliability and maintaining system stability. Mechanical power quantifies the rate of energy conversion into electricity, whereas power flow represents the amount of electrical energy exchanged across areas. The rotor angular frequency corresponds to the generator shaft speed, and the governor time constant reflects the governor's response to load fluctuations. The frequency or load variation denotes the system's reaction to changes in demand.

Table 2. Notation and descriptions[14]

Symbol	**definition**
ω	Rotor angular speed.
M_i	Aggregate inertia associated with area i^{th}.
P_{mech}	Shaft output power delivered mechanically.
P_v	Setting of the steam valve (valve opening).
T_{ch}	Prime-mover time constant.
R^f	Droop coefficient.
D_i	Load-damping coefficient
T_g	Governor time constant.
T_{ij}	Synchronizing coefficient between area i and area j.
$P_{\text{tie},ij}$	Tie-line power transfer from area i and area j.
$P_{\text{tie},i}$	Net tie-line exchange of area i.

Such parameters are commonly used in power system studies, including transient stability and frequency response analyses, to confirm the ability of the system to withstand disturbances. In the context of the proposed multi-area power model (1), the main objective is to establish a distributed control strategy that preserves closed-loop stability across all interconnected regions. Here, $\mathcal{J}_n$ defines the set of neighboring subsystems indexed by j. The control framework uses output feedback from each subsystem to compute the corresponding control input at each time step, thereby ensuring overall system stability. In the context of the model described in (1), the objective is to design an observer-based control scheme that ensures closed-loop stability across all interconnected areas within the power network. Here, N denotes the set of interconnected areas, where each agent

is indexed by j. The distributed observer-based controller aims to sustain system stability and tracking performance within the multi-area power system illustrated in **Figure 1**.

3.1. The communication effects

The sampled measurement signal $\mathcal{Y}_{is}(k)$ is processed by a logarithmic quantization module, yielding the quantized measurement affected by the quantization uncertainty Δq_k. Quantization levels are structured on a log scale:

$$\mathcal{Q}_v = \{\pm\mu_j,\ \mu_j = \kappa^j \mu_b,\ j = 0, \pm1, \pm2, \ldots\} \cup \{0\},\ 0 < \kappa < 1,\ \mu_b > 0$$

In which κ and $Q_\ell(.)$ denote the base ratio and the function of the logarithmic quantizer. The latter can be prescribed as:[13]

$$Q_\ell(\eta) = \begin{cases} \mu_j, & \text{if } \mu_j^- < \eta \le \mu_j^+, \\ 0, & \text{if } \eta = 0, \\ -Q_\ell(-\eta), & \text{if } \eta < 0 \end{cases} \tag{2}$$

where $\omega_q = \frac{1-\kappa}{1+\kappa}$, $\mu_j^- = \frac{\mu_j}{1+\omega_q}$, $\mu_j^+ = \frac{\mu_j}{1-\omega_q}$. The quantizer impact is bounded by the density parameter:

$$Q_\ell(\eta) = \big(1 + \Delta q_k(\eta)\big)\eta, \qquad \|\Delta q_k(\eta)\| \le \omega_q, \quad \forall \eta. \tag{3}$$

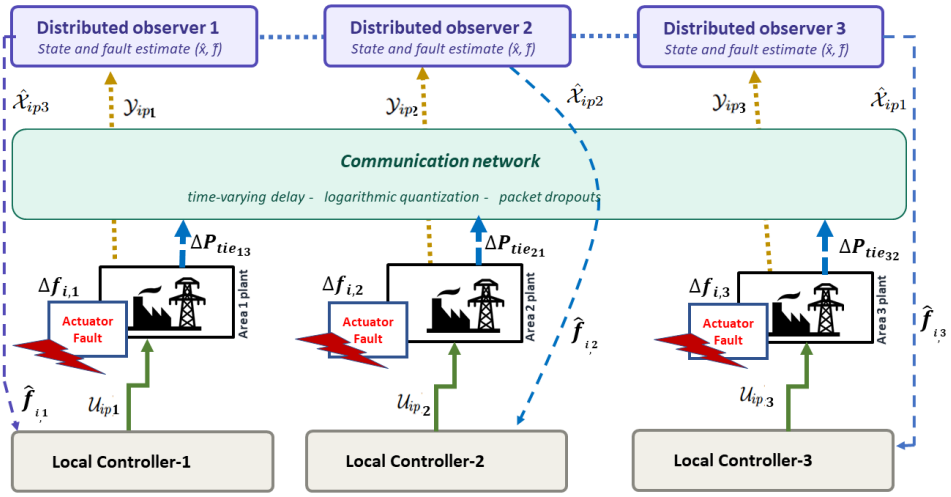


Figure 1. Corresponding schematic for a three-area configuration

The implementation of networked communication systems (NCS) makes the system vulnerable to malfunction at any node due to several aspects such as actuator faults, communication constraints, signal drops, time delays, quantization, and component failures. Thus, both the output and the actuating signals are affected by the faults and time delay. To incorporate the influence of quantization and time delay, the measured signal received by the distributed observer is expressed as follows:

$$\begin{aligned} \mathcal{Y}_{is}(k) &= (1 + \Delta q_k)\mathcal{Y}_{ip}(k - \tau_s^k) \\ &= (1 + \Delta q_k) C_{ip} \mathcal{X}_{ip}(k - \tau_s^k) \end{aligned} \tag{4}$$

where $\tau_s^k \in \{\tau_{\min}, \ldots, \tau_{\max}\}$denotes the delay in the output signal with $0 \le \tau_{\min} \le \tau_{\max}$. The delay process is selected to be a prescribed bounded time-varying delay, and the analysis does not depend on a probabilistic model.

3.2. Actuator fault modeling and compensation

The implementation of networked communications makes the MAIPs vulnerable to sensing-channel communication constraints and actuator-side faults. In this study, the controller-to-actuator network is modeled to be free from communication delay and quantization. The actuator fault is modeled as an additive actuator-side signal that modifies the actual input applied to the plant, and their effects are subsequently embedded in the measurement signal received by the distributed observer. Let the nominal controller be defined as $\mathcal{U}_{ip}(k) = -K\hat{\mathcal{X}}_{ip}(k)$ to stabilize the system in the absence of fault impacts. When an actuator-side fault $f_i(k)$ occurs in area i, the input applied to the plant is expressed as

$$\begin{aligned} \mathcal{U}_{ip}^{\mathrm{F}}(k) &= \mathcal{U}_{ip}(k) + f_i(k) \\ &= -K\hat{\mathcal{X}}_{ip}(k) + f_i(k) \end{aligned} \tag{5}$$

where $\mathcal{U}_{ip}^{\mathrm{F}}(k)$ denotes the uncompensated faulty plant input. Let $f_i(k)$ be the faulty signal affecting the actuator of area i, and $\hat{f}_i(k)$ represent the RBF-NN-based estimate of the actuator fault for area i. To compensate for the actuator influence while sustaining the prescribed performance of the system (1), the proposed controller design incorporates a fault compensation signal. The corresponding fault-compensating control law is given by:

$$\begin{aligned}\mathcal{U}_{ia}(k) &= \mathcal{U}_{ip}^{\mathrm{F}}(k) - \hat{f}_i(k) \\ &= -K\hat{\mathcal{X}}_{ip}(k) + f_i(k) - \hat{f}_i(k) \\ &= -K\hat{\mathcal{X}}_{ip}(k) - \mathcal{E}_{f,i}(k), \end{aligned} \tag{6}$$

Let $\mathcal{U}_{ia}(k)$ denote the actuator-applied input, and $\mathcal{E}_{f,i}(k) = \hat{f}_i(k) - f_i(k)$ denote the fault-estimation error. $\mathcal{E}_{f,i}(k) \to 0$ based on accurate estimation of $\hat{f}_i(k)$, and effective compensation is achieved for $f_i(k)$.

Assumption 1 (Bounded actuator faults)**.** *For each area $i \in \{1, \ldots, N\}$, the unknown actuator-fault signal $f_i : \mathbb{N} \to \mathbb{R}^m$ satisfies the following boundedness conditions: there exist known positive constants ν_f and ν_{df} such that*

$$\|f_i(k)\| \le \nu_f, \quad \|f_i(k+1) - f_i(k)\| \le \nu_{df}, \ \forall\, k \ge 0, \tag{7}$$

where $\|\cdot\|$ denotes the Euclidean norm.

Remark 1. *Note that the assumption of bounded $f_i(k)$ is reasonable, as the control input range is bounded. The unbounded actuator faults can be detected and filtered by conventional anomaly detection protocols and simple filters. Moreover, the assumption of bounded $f_i(k+1)$ is acceptable when ν_{df} is regarded as the Lipschitz constant.*

Let $T_i \in \mathbb{R}^{(n+m)\times(n+m)}$ and $N_i \in \mathbb{R}^{(n+m)\times q}$ be the parameter matrices to be designed. With $\bar{C}_i \in \mathbb{R}^{q\times(n+m)}$, matrices T_i and N_i are required to satisfy the constraint:

$$T_i + N_i\bar{C}_i = I_{n+m}, \tag{8}$$

where I_{n+m} denotes the $(n+m)\times(n+m)$ dimensional identity matrix.

3.3. Radial-basis-function based neural network

RBF-NN is a three-layer feedforward architecture with a simple configuration, rapid training, and reliable performance. It has been proven to approximate unknown nonlinear dynamics with satisfactory accuracy. For facilitating the proposed controller design, the RBF-NN is used to approximate the actuator faults $f_i(k)$. Suppose that

$$G_j\big(\mathcal{X}_{ip}(k)\big) = \exp\left(\frac{-\|\mathcal{X}_{ip}(k) - v_{i,j}\|^2}{2\sigma_j^2}\right), \quad j = 1, 2, \ldots, m, \tag{9}$$

where $\mathcal{X}_i(k)$ is the NN input, and m is the number of NN nodes. $v_{i,j}$ is the center and $\sigma_j > 0$ is width of the function $G_i(\mathcal{X}_i(k))$, respectively. Define the radial basis function (RBF) as

$$\begin{aligned}G_i(\mathcal{X}_i(k)) = [&G_1(\mathcal{X}_i(k)), G_2(\mathcal{X}_i(k)), \ldots, \\ &G_m(\mathcal{X}_i(k))]^T\end{aligned} \tag{10}$$

RBF-NN has been widely used to approximate unknown nonlinear functions. Therefore, a class of linearly parameterized NNs is adopted to approximate the continuous function $f(\mathcal{X}_i)$, and can be expressed as

$$\begin{aligned}&f_i(\mathcal{X}_{ip}(k)) = W_i^{*\top} G_i(\mathcal{X}_{ip}(k)) + \mathbf{e}_{n,i}(\mathcal{X}_{ip}(k)), \\ &\|\mathbf{e}_{n,i}(\cdot)\| \le \bar{\mathbf{e}}_{n,i}\end{aligned} \tag{11}$$

$W_i^* \in \mathbb{R}^{m\times q}$ is an ideal weight matrix. $\mathbf{e}_{n,i}(\mathcal{X}_{ip}(k))$ denotes the NN approximation error, where $\bar{\mathbf{e}}_{n,i} > 0$, and $\|G_i(\cdot)\| \le G_{\max}$ with a positive constant $G_{\max}$.[35] The local output residual drives the adaptation mechanism

$$\mathbf{e}_{n,i}(\mathcal{X}_{ip}(k)) = \mathcal{Y}_{ip}(k) - C_{ip}\hat{\mathcal{X}}_{ip}(k), \tag{12}$$

where $\mathcal{Y}_{ip}(k)$ denotes the measured output of area i, and $C_{ip}\hat{\mathcal{X}}_{ip}(k)$ represents the estimated output generated by the observer. To approximate the actuator faults $f_i(\mathcal{X}_{ip}(k))$, the adaptive law should be properly designed. According to the output of the RBF-NN, we have

$$\hat{f}_i(\mathcal{X}_{ip}) = \hat{W}_i(k)^\top G_i(\mathcal{X}_{ip}(k)) \tag{13}$$

$\hat{W}_i(k) \in \mathbb{R}^{m\times q}$ is the adaptive estimate of the ideal weight matrix W_i^* in (11). The adaptation update law for the neural-network weights is chosen as

$$\begin{aligned}\hat{W}_i(k+1) = \mathrm{Proj}\Big(&\hat{W}_i(k) + \\ &\Gamma_i G_i(\mathcal{X}_{ip}(k))\mathbf{e}_{n,i}^\top(\mathcal{X}_{ip}(k)) - \kappa_i\Gamma_i\hat{W}_i(k)\Big),\end{aligned} \tag{14}$$

the gradient term $\Gamma_i\Phi\mathbf{e}_{n,i}^\top(\mathcal{X}_{ip}(k))$ ensures Lyapunov-aligned descent against the augmented observer error; the σ-leakage $-\kappa_i\Gamma_i\hat{W}_i$ ensures exponential forgetting that bounds the weight drift under approximation error ε_i; the projection Proj ensures the hard bound $|\hat{W}_i(k)|_F \le \bar{w}$ for all $k \ge 0$.

Remark 2. *The adaptation law* (15) *depends only on the locally measurable output residual $\mathbf{e}_{n,i}(\mathcal{X}ip(k))$ and the observer state available in area i. Unlike gradient laws based on the fault*

-estimation residual, the true fault $f_i(k)$ does not have to be known.

Define the neural-network weight-estimation error as

$$\tilde{W}_i(k) = W_i^* - \hat{W}_i(k) \tag{15}$$

We then construct the following approximation error:

$$\mathcal{E}_{f,i}(k) = f_i(k) - \hat{f}_i(k) = \tilde{W}_i^\top(k) G_i(\mathcal{X}_{ip}(k)) + \mathbf{e}_{n,i}(\mathcal{X}ip(k)). \tag{16}$$

which gives the adaptive estimation of actuator faults $f_i(k)$.

3.4. Projection adaptive law

Lemma 1.[36] Given matrices $\mathcal{X}_{ip} \in \mathbb{R}^{a\times b}$, $\mathcal{Y}_{ip} \in \mathbb{R}^{b\times c}$, and $\mathcal{Z}_{ip} \in \mathbb{R}^{a\times c}$, if $\text{rank}(\mathcal{Y}_{ip}) = c$, then the general solution of $\mathcal{X}_{ip}\mathcal{Y}_{ip} = \mathcal{Z}_{ip}$ is

$$\mathcal{X}_{ip} = \mathcal{Z}_{ip}\mathcal{Y}_{ip}^+ + \mathcal{H}\left[\mathcal{I}_b - \mathcal{Y}_{ip}\mathcal{Y}_{ip}^+\right], \tag{17}$$

where $\mathcal{H} \in \mathbb{R}^{a\times b}$ is an arbitrary matrix, and $\mathcal{Y}_{ip}^+$ is the pseudo-inverse matrix of $\mathcal{Y}_{ip}$.

By **Equation (17)**, T_i and N_i satisfy $T_i + N_i\bar{C}_i = I_{n+m}$. Applying Lemma 1 to **Equation (17)**, yields:

$$\begin{bmatrix} T_i \\ N_i \end{bmatrix} = \begin{bmatrix} I_{n+m} \\ 0 \end{bmatrix} \bar{C}_i^+ + S\left[I_{n+m} - \bar{C}_i\bar{C}_i^+\right], \tag{18}$$

where $S \in \mathbb{R}^{(n+m)\times(n+m+q)}$ is an arbitrary matrix.

After parameter matrices T_i and N_i are determined, **Equations (6)** and **(8)** can be used to obtain the adaptive algorithm for parameter estimation:

$$\dot{\hat{\theta}}_i = \Gamma_i \bar{\phi}_i^T(\hat{\bar{\mathcal{X}}}_{ip}, \bar{\mathcal{U}}_{ip}, \bar{\mathcal{Y}}_{ip}) R_i^T(\bar{\mathcal{Y}}_{ip} - \hat{\bar{\mathcal{Y}}}_{ip}) \tag{19}$$

$\Gamma_i = \Gamma_i^T > 0$ is the adaptation gain, which is selected by trial and error method to ensure that $\dot{\hat{\theta}}$ does not grow unbounded[37]. To facilitate concurrent estimation capability of states and fault dynamics, an augmented state vector $\bar{\mathcal{X}}_{ip}(k) = [\mathcal{X}_{ip}(k);\ \mathcal{E}_{f,i}(\mathcal{X}_{ip}(k))]$ is introduced, leading to

$$\begin{aligned} \bar{\mathcal{X}}_{ip}(k+1) &= A_{ii}\bar{\mathcal{X}}_{ip}(k) + B_i\bar{\mathcal{U}}_{ip}(k) \\ &+ \mathcal{N}_{f,i}(\bar{\mathcal{X}}_{ip}(k)) \\ &+ \bar{\psi}_{ip}(\bar{\mathcal{X}}_{ip}, \bar{\mathcal{Y}}_{ip}, \bar{\mathcal{U}}_{ip})\bar{\theta}_i(k) \\ \bar{\mathcal{Y}}_{ip}(k) &= C_i\bar{\mathcal{X}}_{ip}(k). \end{aligned} \tag{20}$$

By substituting (1) and (16), the augmented system matrices are obtained as

$$A_{ii} = \begin{bmatrix} A_{ip} & B_{ip} \\ 0 & I_m \end{bmatrix}, B_i = \begin{bmatrix} B_{ip} \\ 0 \end{bmatrix},$$

$$\mathcal{N}_{f,i}(\bar{\mathcal{X}}_{ip}(k)) = \begin{bmatrix} \mathcal{D}_{ip}W_{ip}(k) \\ \Delta\mathcal{E}_{f,i}(k) \end{bmatrix},$$

$$\bar{\psi}_{ip} = \begin{bmatrix} \psi_{ip} \\ 0 \end{bmatrix}, \quad C_i = \begin{bmatrix} C_{ip} & 0 \end{bmatrix},$$

where $\mathcal{N}_{f,i}(\bar{\mathcal{X}}_{ip}(k))$ represents the lumped disturbance/fault-increment term. The following augmentation system estimates actuator faults and dynamic states simultaneously:

$$\begin{aligned} \bar{\mathcal{X}}_{ip}(k+1) &= T_iA_{ii}\bar{\mathcal{X}}_{ip}(k) + T_iB_i\bar{\mathcal{U}}_{ip}(k) \\ &+ T_i\mathcal{N}_{f,i}(\bar{\mathcal{X}}_{ip}(k)) \\ &+ T_i\bar{\psi}_{ip}(\bar{\mathcal{X}}_{ip}, \bar{\mathcal{Y}}_{ip}, \bar{\mathcal{U}}_{ip})\bar{\theta}_i(k) \\ &= \bar{A}_{ii}\bar{\mathcal{X}}_i(k) \\ &+ \bar{B}_i\bar{\mathcal{U}}_{ip}(k) + \bar{\mathcal{N}}_f(\bar{\mathcal{X}}_{ip}(k)) \\ &+ \bar{\psi}_i(\bar{\mathcal{X}}_{ip}, \bar{\mathcal{Y}}_{ip}, \bar{\mathcal{U}}_{ip})\bar{\theta}_i(k) \\ \bar{\mathcal{Y}}_{ip}(k) &= T_iC_i\bar{\mathcal{X}}_{ip}(k) \\ &= \bar{C}_i\bar{\mathcal{X}}_{ip}(k) \end{aligned} \tag{21}$$

Remark 3. *Theorem 1 establishes the stability and performance of the distributed observer error dynamics without requiring individual convergence of the RBF-NN weights. The neural-network weights are uniformly bounded, i.e., $\|\hat{w}_{n,i}(k)\| \le \bar{w}_{n,i}$ for all $k \ge 0$, as enforced by the projection adaptive law. Together with bounded RBF basis functions and a bounded NN approximation error, this ensures that the residual fault-estimation term $\Delta f_i(k) \triangleq f_i(k+1) - f_i(k)$ is bounded, see assumption 1. Thus, this term can be treated as part of the disturbance affecting the observer-error system. Consequently, the theorem ensures exponential mean-square stability for zero lumped disturbance and the prescribed ℓ_2-gain performance within $\ell_2[0,\infty)$.*

3.5. State observer design

To estimate the unknown parameters in area i, a state observer is developed that leverages information from the area p while accounting for the communication constraints affecting area i. The observer formulation is illustrated below. Accordingly, the observer associated with system (1) takes the following form:

$$\begin{cases} \mathcal{Z}_i(k+1) = T_iA_{ii}\,\hat{\bar{\mathcal{X}}}_{ip}(k) + T_iB_i\,\bar{\mathcal{U}}_{ip}(k) \\ \qquad\qquad + T_i\bar{\psi}_{ip}\big(\bar{\mathcal{X}}_{ip}, \bar{\mathcal{Y}}_{ip}, \bar{\mathcal{U}}_{ip}\big)\,\bar{\theta}_i(k) \\ \qquad\qquad + L_i\big(\bar{\mathcal{Y}}_{ip}(k) - \bar{C}_i\,\bar{\mathcal{X}}_{ip}(k)\big), \\ \hat{\bar{\mathcal{X}}}_{ip}(k) = \mathcal{Z}_i(k) + N_i\,\bar{\mathcal{Y}}_{ip}(k) \end{cases} \tag{22}$$

$\mathcal{Z}_i(k)$ is an intermediate state vector $\bar{\mathcal{X}}_{ip}(k)$, $\hat{\bar{\mathcal{X}}}_{ip}(k) \in \mathbb{R}^{(n+m)}$ is the estimated vector of the augmented state. Considering the formulas (19) and (22), the following estimator is obtained:

$$\begin{aligned} \hat{\bar{\mathcal{X}}}_{ip}(k+1) &= \bar{A}_{ii}\hat{\bar{\mathcal{X}}}_{ip}(k) + \bar{B}_i\bar{\mathcal{U}}_{ip}(k) \\ &+ N_i\mathcal{Y}_{ip}(k+1) \\ &+ \bar{\psi}_i(\bar{\mathcal{X}}_{ip}, \bar{\mathcal{Y}}_{ip}, \bar{\mathcal{U}}_{ip})\bar{\theta}_i(k) \\ &+ L_i\big(\bar{\mathcal{Y}}_{ip}(k) - \bar{C}_i\hat{\bar{\mathcal{X}}}_{ip}(k)\big) \end{aligned} \tag{23}$$

Obviously, observer (23) has more design degrees of freedom than the Luenberger observer.

In summary, the proposed observer structure follows a two-step design: first, actuator fault dynamics are integrated into an augmented system model (1). Second, a distributed observer is designed to utilize local measurements and neighbors' estimates while explicitly accounting for quantization and time-varying delays (21). This structure is further enhanced by a radial basis function neural network (RBF-NN) that approximates unknown nonlinear fault effects.

Remark 4. *Conventional model-based estimation methods, such as observer-based schemes and Kalman filters, are primarily designed to be effective at attenuating abnormal signals rather than to isolate fault signatures. As a result, the performance of these methods depends heavily on the accuracy of the models used, and they generally cannot distinguish faults from disturbances or noise. In contrast, a radial basis function neural network (RBF-NN) can learn fault patterns directly from data after training, making it effective in separating the actual fault effects from disturbances and noise.*

3.6. Derivation of error dynamics

The estimation error is defined as $\mathcal{E}_{\bar{x}}i(k) = \bar{\mathcal{X}}_{ip}(k) - \hat{\bar{\mathcal{X}}}_{ip}(k)$. The following error dynamics are obtained by subtracting the observer dynamics from the system equation:

$$\begin{aligned}\mathcal{E}_{\bar{x}i}(k+1) &= \bar{\mathcal{X}}_{ip}(k+1) - \hat{\bar{\mathcal{X}}}_{ip}(k+1)\\ &= \bar{A}_{ii}\left(\bar{\mathcal{X}}_{ip}(k) - \hat{\bar{\mathcal{X}}}_{ip}(k)\right) + \bar{\mathcal{N}}_f(\mathcal{X}_{ip}(k))\\ &\quad - L_i\Big[(1+\Delta q_k)\bar{C}_i\bar{\mathcal{X}}_{ip}(k-\tau_s^k)\\ &\quad - (1+\Delta q_k)\bar{C}_i\hat{\bar{\mathcal{X}}}_{ip}(k-\tau_s^k)\Big]\\ &\quad - N_i\bar{\mathcal{Y}}_{ip}(k+1)\\ &= \bar{A}_{ii}\mathcal{E}_{\bar{x}i}(k) + \bar{\mathcal{N}}_f(\mathcal{X}_{ip}(k))\\ &\quad - (1+\Delta q_k)L_i\bar{C}_i\mathcal{E}_{\bar{x}i}(k-\tau_s^k)\\ &\quad - N_i\bar{\mathcal{Y}}_{ip}(k+1)\end{aligned} \tag{24}$$

The disturbance acting on the distributed observer-error dynamics is defined as $\omega_i(k) := \bar{\mathcal{N}}_{f,i}(\bar{\mathcal{X}}_{ip}(k)) - N_i\bar{\mathcal{Y}}_{ip}(k+1)$. Then

$$\begin{aligned}\mathcal{E}_{\bar{x}i}(k+1) &= \bar{A}_{ii}\mathcal{E}_{\bar{x}i}(k)\\ &\quad - (1+\Delta q_k)L_i\bar{C}_i\mathcal{E}_{\bar{x}i}(k) + \omega_i(k)\end{aligned} \tag{25}$$

Utilizing the error dynamics in (24), the subsequent section formulates main results on the distributed observer gains to ensure that the estimation-error framework is exponentially stable and attains a specified ℓ_2 performance within constraints.

4. Stability analysis

This section presents sufficient conditions for the observer dynamic systems described in (24) to achieve exponential mean-square stability and meet a specified ℓ_2 gain bound. The results are organized into two main theorems.Theorem 1 establishes the stability analysis and performance requirements using distributed observer gains. Theorem, 2 reformulates the stability and performance conditions into the form of a convex linear matrix inequality (LMI). To analyze the stability of the error dynamics 24, the following Lyapunov-Krasovskii functional is considered:

$$\begin{aligned}V(\mathcal{E}_{\bar{x}i}(k)) &= \sum_{i=1}^{3} V_i(\mathcal{E}_{\bar{x}i}(k)),\\ V_1(\mathcal{E}_{\bar{x}i}(k)) &= \sum_{j=1}^{2} \mathcal{E}_{\bar{x}i}^T(k)P_i\mathcal{E}_{\bar{x}i}(k),\\ V_2(\mathcal{E}_{\bar{x}i}(k)) &= \sum_{j=1}^{2}\sum_{i=k-\tau_s^k}^{k-1} \mathcal{E}_{\bar{x}i}^T(i)Q_j\mathcal{E}_{\bar{x}i}(i),\\ Q_j &= Q_j^T > 0,\\ V_3(\mathcal{E}_{\bar{x}i}(k)) &= \sum_{j=1}^{2}\sum_{\ell=-\tau_s^-+1}^{-\tau_s^++2}\sum_{i=k+\ell-1}^{k-1} \mathcal{E}_{\bar{x}i}^T(i)Q_j\mathcal{E}_{\bar{x}i}(i)\end{aligned} \tag{26}$$

where $P_i > 0$. It can be easily confirmed that positive real scalars μ and v exist such that $\mu\|e\|^2 \le V(\mathcal{E}_{\bar{x}i}(k)) \le v\|\mathcal{E}_{\bar{x}i}(k)\|^2$. The subsequent analysis defines a criterion under which the error system (24) is assuredly asymptotically stable.

Remark 5. *To establish exponential stability of the closed-loop system, we construct a Lyapunov function $V(\mathcal{E}_{\bar{x}i}(k))$ as defined in **Equation (23)**, which aggregates multiple quadratic terms that account for state delays and fault effects. The sufficient condition for stability is that the forward difference of the Lyapunov function,*

$$\Delta V(\mathcal{E}_{\bar{x}i}(k)) = V(\mathcal{E}_{\bar{x}i}(k+1)) - V(\mathcal{E}_{\bar{x}i}(k)),$$

*is negative definite. To this end, we derive the matrix inequality in **Equation (27)**, where $\Lambda_j < 0$ ensures that all the individual contributions to $\Delta V(\mathcal{E}_{\bar{x}i}(k))$ are strictly negative. This inequality is obtained by substituting the system dynamics into the difference $\Delta V(\mathcal{E}_{\bar{x}}i)$, and applying bounds and norm properties on delayed terms and fault perturbations. Suppose the LMI condition in **Equation (26)** is feasible. In this case, the Lyapunov function decreases along the system trajectories,*

implying exponential mean-square stability of the closed-loop system under bounded actuator faults and communication delays.

Theorem 1. *Consider the error system (24) under bounded time-varying $\tau_s^k \in [\tau_s^-, \tau_s^+]$ and quantization uncertainty Δ_k, for a given estimator gain L_i. If there exist matrices $P_i > 0$, $Q_j = Q_j^T > 0$, and slack matrices $\mathcal{S}_i$, $\mathcal{K}_i$, and $\mathcal{M}_i$ such that $\Xi_j < 0$ holds for $j = 1, 2$, then the error system is asymptotically stable and achieves $\|\tilde{z}(k)\|_2 < \gamma\|w(k)\|_2$.*

$$\Xi_j = \begin{bmatrix} \Xi_{1j} & \Xi_{2j} & G^T \\ \bullet & -\gamma^2 I - \Upsilon_{j4} & 0 \\ \bullet & \bullet & -I \end{bmatrix} < 0,$$

$$\Xi_{1j} = \begin{bmatrix} \Psi_j + \Upsilon_{j1} & -\mathcal{K}_i + -\mathcal{S}_i^T & -\mathcal{K}_i + \mathcal{M}_i^T + \Upsilon_{j6} \\ \bullet & -\mathcal{S}_i - \mathcal{S}_i^T - \sigma_j Q_j & -\mathcal{S}_i + \mathcal{M}_i^T \\ \bullet & \bullet & -\mathcal{M}_i - \mathcal{M}_i^T - \Upsilon_{j3} \end{bmatrix}, \quad (27)$$

$$\Xi_{2j} = \begin{bmatrix} \Upsilon_{j2} \\ 0 \\ \Upsilon_{j5} \end{bmatrix},$$

$$\mathbf{E}(k) = \mathrm{col}\big(\mathcal{E}_{\bar{x}1}(k), \ldots, \mathcal{E}_{\bar{x}n}(k)\big),$$
$$\mathbf{P} = \mathrm{blkdiag}(P_1, \ldots, P_n),$$
$$\mathbf{Q}_j = \mathrm{blkdiag}(Q_{j,1}, \ldots, Q_{j,n}),$$
$$\bar{\mathbf{A}} = \mathrm{blkdiag}(\bar{A}_1, \ldots, \bar{A}_n),$$
$$\bar{\mathbf{B}} = \mathrm{blkdiag}(\bar{B}_1, \ldots, \bar{B}_n),$$
$$\bar{\mathbf{C}} = \mathrm{blkdiag}(\bar{C}_1, \ldots, \bar{C}_n),$$
$$\mathbf{L} = \mathrm{blkdiag}(L_1, \ldots, L_n),$$
$$\mathcal{K} = \mathrm{blkdiag}(\mathcal{K}_1, \ldots, \mathcal{K}_n),$$
$$\mathcal{S} = \mathrm{blkdiag}(\mathcal{S}_1, \ldots, \mathcal{S}_n)$$
$$\Psi_j = \mathrm{blkdiag}_i\Big(- P_i + \sigma_j(1 + \tau_s^+ - \tau_s^-) Q_{j,i} + \mathcal{K}_i + \mathcal{K}_i^T\Big),$$
$$\Upsilon_{j1} = \mathrm{blkdiag}_i\Big(\big(\bar{A}_i - (I + \Delta_k)L_i\bar{C}_i\big)^T P_i\big(\bar{A}_i - (I + \Delta_k)L_i\bar{C}_i\big)\Big),$$
$$\Upsilon_{j2} = \mathrm{blkdiag}_i\Big(\big(\bar{A}_i - (I + \Delta_k)L_i\bar{C}_i\big)^T P_i\, \bar{B}_i\Big),$$
$$\Upsilon_{j3} = \mathrm{blkdiag}_i\big(\bar{C}_i^T L_i^T P_i L_i \bar{C}_i\big),$$
$$\Upsilon_{j4} = \mathrm{blkdiag}_i\big(\bar{B}_i^T P_i \bar{B}_i\big),$$
$$\Upsilon_{j5} = \mathrm{blkdiag}_i\big(\bar{B}_i^T P_i L_i \bar{C}_i\big), \quad (28)$$
$$\Upsilon_{j6} = \mathrm{blkdiag}_i\Big(\big(\bar{A}_i - (I + \Delta_k)L_i\bar{C}_i\big)^T P_i L_i \bar{C}_i\Big).$$

Proof: To analyze observer stability, especially under network-induced delays, following,[38] we define

$$\mathcal{E}_{\bar{x}i}(k - \tau_s^k) = \mathcal{E}_{\bar{x}i}(k) - \sum_{l=k-\tau_s^k}^{k-1} y(l) = \mathcal{E}_{\bar{x}i}(k) - \lambda_i(k) \quad (29)$$

Consequently, the error dynamics described in (24) can be rewritten as:

$$\begin{aligned} \mathcal{E}_{\bar{x}i}(k+1) = &\Big(\bar{A}_{ii} - (1 + \Delta q_k)L_i\bar{C}_i\Big)\mathcal{E}_{\bar{x}i}(k) \\ &+ (1 + \Delta q_k)L_i\bar{C}_i\lambda_i(k) \\ &+ \bar{\mathcal{N}}_f(\mathcal{X}_{ip}(k)) \\ &- N_i\bar{\mathcal{Y}}_{ip}(k+1) \end{aligned} \quad (30)$$

By evaluating the forward difference of $V_1(\mathcal{E}_{\bar{x}i}(k))$ along the trajectories of system (30) under (28), we obtain:

$$\begin{aligned} \mathbb{E}\left[\Delta V_1(\mathcal{E}_{\bar{x}i}(k))\right] =& \mathbb{E}\left[V_1(\mathcal{E}_{\bar{x}i}(k+1))\right] - V_1(\mathcal{E}_{\bar{x}i}(k)) \\ =& \sum_{j=1}^{2}[\mathcal{E}_{\bar{x}i}^T(k)\left[\Upsilon_{j1} - P_i\right]\mathcal{E}_{\bar{x}i}(k) \\ &- 2\mathcal{E}_{\bar{x}i}^T(k)\Upsilon_{j2}\lambda_i(k) \\ &+ \lambda_i^T(k)\Upsilon_{j3}\lambda_i(k). \\ &+ w^T\Upsilon_{j4}w \\ &+ 2w^T\bar{B}_i^T P_i L_i\bar{C}_i\lambda_i(k)] \end{aligned} \quad (31)$$

A straightforward computation gives

$$\begin{aligned} \mathbb{E}\left[\Delta V_2(\mathcal{E}_{\bar{x}i}(k)\right] =& \sum_{j=1}^{2}\sigma_j\left[\sum_{l=k+1-\tau_{k+1}^s}^{k}\mathcal{E}_{\bar{x}i}^T(l)Q_j\mathcal{E}_{\bar{x}i}(l)\right. \\ &- \sum_{l=k-\tau_s^k}^{k-1}\mathcal{E}_{\bar{x}i}^T(l)Q_j\mathcal{E}_{\bar{x}i}(l) \\ =& \mathcal{E}_{\bar{x}i}^T(k)Q\mathcal{E}_{\bar{x}i}(k) \\ &- \mathcal{E}_{\bar{x}i}\left(-\tau_s^k\right)Q_j\mathcal{E}_{\bar{x}i}\left(-\tau_s^k\right) \\ &+ \sum_{l=k+1-\tau_{k+1}^s}^{k-1}\mathcal{E}_{\bar{x}i}^T(l)Q_j\mathcal{E}_{\bar{x}i}(l) \\ &\left.- \sum_{l=k+1-\tau_s^k}^{k-1}\mathcal{E}_{\bar{x}i}(l)Q_j\mathcal{E}_{\bar{x}i}(l)\right] \end{aligned} \quad (32)$$

In view of

$$\sum_{l=k+1-\tau_{k+1}^{s}}^{k-1}\mathcal{E}_{\bar{x}i}^{T}(l)Q_j\mathcal{E}_{\bar{x}i}(l)=\sum_{l=k+1-\tau_{k+1}^{s}}^{k-\tau_s^k}\mathcal{E}_{\bar{x}i}^{T}(l)Q_j\mathcal{E}_{\bar{x}i}(l)+\sum_{l=k+1-\tau_s^k}^{k-1}\mathcal{E}_{\bar{x}i}^{T}(l)Q_j\mathcal{E}_{\bar{x}i}(l)\leqslant\sum_{l=k+1-\tau_s^k}^{k-1}\mathcal{E}_{\bar{x}i}^{T}(l)Q_j\mathcal{E}_{\bar{x}i}(l)+\sum_{l=k+1-\tau_s^+}^{k-\tau_s^-}\mathcal{E}_{\bar{x}i}^{T}(l)Q_j\mathcal{E}_{\bar{x}i}(l) \quad (33)$$

Hence, the following relation holds:

$$\mathbb{E}\left[\Delta V_2(\mathcal{E}_{\bar{x}i}(k))\right]\leqslant\sum_{j=1}^{2}\sigma_j[\mathcal{E}_{\bar{x}i}^{T}(k)Q_j\mathcal{E}_{\bar{x}i}(k)-\mathcal{E}_{\bar{x}i}^{T}(k-\tau_s^k)Q_j\mathcal{E}_{\bar{x}i}\left(k-\tau_s^k\right)+\sum_{l=k+1-\tau_s^+}^{k-\tau_s^-}\mathcal{E}_{\bar{x}i}^{T}(l)Q_j\mathcal{E}_{\bar{x}i}(l)] \quad (34)$$

Therefore,

$$\mathbb{E}\left[\Delta V_3(\mathcal{E}_{\bar{x}i}(k))\right]=\sum_{j=1}^{2}\sigma_j[\sum_{\ell=-\tau_s^++2}^{-\tau_s^-+1}[\mathcal{E}_{\bar{x}i}^{T}(k)Q_j\mathcal{E}_{\bar{x}i}(k)-\mathcal{E}_{\bar{x}i}^{T}(k+\ell-1)Q_j\mathcal{E}_{\bar{x}i}(k+\ell-1)]]=\sum_{j=1}^{2}\sigma_j[\left(\tau_s^+-\tau_s^-\right)\mathcal{E}_{\bar{x}i}^{T}(k)Q_j\mathcal{E}_{\bar{x}i}(k)-\sum_{l=k+1-\tau_s^+}^{k-\tau_s^-}\mathcal{E}_{\bar{x}i}^{T}(l)Q_j\mathcal{E}_{\bar{x}i}(l)] \quad (35)$$

Equation (29) yields $\mathcal{E}_{\bar{x}i}(k)-\mathcal{E}_{\bar{x}i}\left(-\tau_s^k\right)-\lambda_i(k)=0$. Hence, for any admissible dimensions of $R,\mathcal{S}_1$ and M_1, the system satisfies the following equality:

$$2\left[\mathcal{E}_{\bar{x}i}^{T}(k)\mathcal{K}_i+\mathcal{E}_{\bar{x}i}^{T}(k-\tau_s^k)\mathcal{S}_i+\lambda_i^{T}(k)\mathcal{M}_i\right]\left[\mathcal{E}_{\bar{x}i}(k)-\mathcal{E}_{\bar{x}i}\left(k-\tau_s^k\right)-\lambda_i(k)\right]=0 \quad (36)$$

From the combination of (31)–(36) and (28), it follows that

$$\begin{aligned}\mathbb{E}[\Delta V(\mathcal{E}_{\bar{x}i}(k))]\leqslant&\sum_{j=1}^{2}[\mathcal{E}_{\bar{x}i}^{T}(k)(\Psi_j+\Upsilon_{j1})\mathcal{E}_{\bar{x}i}(k)+\sum_{j=1}^{2}\mathcal{E}_{\bar{x}i}^{T}(k)(-2\mathcal{K}_i+2\mathcal{S}_i^{T})\mathcal{E}_{\bar{x}i}(-\tau_s^k)+\mathcal{E}_{\bar{x}i}^{T}(k)\left(-2\mathcal{K}_i+2\mathcal{M}_i^{T}-2\Upsilon_{j6}\right)\lambda_i(k)+\mathcal{E}_{\bar{x}i}^{T}(k-\tau_s^k)\left(-\mathcal{S}_i-\mathcal{S}_i^{T}-\sigma_jQ_j\right)\xi(k-\tau_s^k)+\mathcal{E}_{\bar{x}i}^{T}(k-\tau_s^k)\left(-2\mathcal{S}_i-2\mathcal{M}_i^{T}\right)\lambda_i(k)+\lambda_i^{T}(k)\left(-\mathcal{M}_i-\mathcal{M}_i^{T}+\Upsilon_{j5}\right)\lambda_i(k)+w^{T}(k)\Upsilon_{j4}w(k)+2w^{T}(k)\Upsilon_{j5}\lambda_i(k)+2\mathcal{E}_{\bar{x}i}^{T}(k)\Upsilon_{j2}w(k)]\\=&\sum_{j=1}^{2}\left[\zeta^{T}(k)\tilde{\Xi}_j\zeta(k)\right]\end{aligned} \quad (37)$$

Here is defined as $\zeta_i(k)=\mathrm{col}\{\mathcal{E}_{x_i}(k),\ \mathcal{E}_{x_i}(k-\tau_s^k),\ \lambda_i(k),\ w_i(k)\}$. and $\tilde{\Xi}_j$ relates to Ξ_j in (28) through Schur complement conditions when $G\equiv 0$. If $\Xi_j<0, j=1,\ldots,2$ holds, then the error system (24) is asymptotically stable. Consider the performance index $J=\sum_0^\infty\left(\tilde{z}^t(k)\tilde{z}(k)-\gamma^2w^t(k)w(k)\right)$. For every nonzero $w(k)\in\ell_2(0,\infty)$ and initial state set to zero $\mathcal{E}_{\bar{x}i}(0)=0$, it follows that

$$\begin{aligned}J=&\sum_{0}^{\infty}(\tilde{z}^t(k)\tilde{z}(s)-\gamma^2w^t(k)w(k)+\Delta V(\mathcal{E}_{\bar{x}i}(k))-\Delta V(\mathcal{E}_{\bar{x}i}(k))) \quad (38)\\\leqslant&\sum_{0}^{\infty}(z^t(k)z(k)-\gamma^2w^t(k)w(k)+\Delta V(\mathcal{E}_{\bar{x}i}(k)) \quad (39)\end{aligned}$$

Continuing the derivation, we obtain $\tilde{z}^t(k)\tilde{z}(k)-\gamma^2w^t(k)w(k)+\Delta V(\mathcal{E}_{\bar{x}i}(k))=\left[\zeta^{T}(k),\quad\tilde{\Xi}_j,\quad\zeta(k)\right]$. From (28), the Schur complement property shows $\tilde{z}^t(s)\tilde{z}(s)-\gamma^2w^t(s)w(s)+\Delta V(\mathcal{E}_{\bar{x}i}(s))<0$ for arbitrary $s\in[0,\infty)$, which indicates that for any nonzero $w(k)\in\ell_2(0,\infty)$

that $J < 0$ holds, yielding $\|\tilde{z}(k)\|_2 < \gamma\|w(k)\|_2$ and thus the proof is finalized.
The estimator design issue can be addressed through the subsequent theorem.

Theorem 2. *If there exist matrices $X_i = X_i^T > 0$, $Z_j = Z_j^T > 0$ for $j = 1, 2$, and free matrices Θ_i, Π_i, Ω_i such that $\hat{\Xi}_j < 0$, then the closed-loop error system (24) is asymptotically stable and achieves ℓ_2-gain $< \gamma_i$. Moreover, the observer gain can be recovered from the change of variables specified below.*

$$\hat{\Xi}_j = \begin{bmatrix} \hat{\Xi}_{1j} & \hat{\Xi}_3 & \hat{\Xi}_4 & 0 \\ \bullet & \hat{\Xi}_{2j} & \hat{\Xi}_6 & 0 \\ \bullet & \bullet & \hat{\Xi}_7 & 0 \\ \bullet & \bullet & \bullet & -\gamma_i^2 I_i \\ \bullet & \bullet & \bullet & \bullet \\ \bullet & \bullet & \bullet & \bullet \end{bmatrix} \begin{bmatrix} X_i G_i^T & \hat{\Xi}_5 \\ 0 & 0 \\ 0 & Y_i^T \\ 0 & X_i \bar{B}_i^T \\ -I_i & 0 \\ \bullet & -X_i \end{bmatrix} < 0, \tag{40}$$

$$\hat{\Xi}_{1j} = -X_i + \sigma_j \left(1 + \tau_s^+ - \tau_s^-\right) Z_j + \Pi_i + \Pi_i^T,$$
$$\hat{\Xi}_{2j} = -\Theta_i - \Theta_i^T - \sigma_j Z_j, \hat{\Xi}_3 = -\Pi_i + \Theta_i^T,$$
$$\hat{\Xi}_4 = -\Pi_i + \Omega_i^T,$$
$$\hat{\Xi}_5 = X_i \bar{A}_{ii}^T - Y_i^T, \hat{\Xi}_6 = -\Theta_i + \Omega_i,$$
$$\hat{\Xi}_7 = -\Omega_i - \Omega_i^T,$$

In addition, the estimator gain can be expressed as $L_i = Y_i X_i^{-1} \bar{C}_i^\dagger$.

Proof: By expanding LMI (27) together with (28) through Schur complements, we obtain

$$\Xi_j = \begin{bmatrix} \Psi_j & -\mathcal{K}_i + \mathcal{S}_i^T & -\mathcal{K}_i + \mathcal{M}_i^T \\ \bullet & -\mathcal{S}_i - \mathcal{S}_i^T - \sigma_j Q_j & -\mathcal{S}_i + \mathcal{M}_i^T \\ \bullet & \bullet & -\mathcal{M}_i - \mathcal{M}_i^T \\ \bullet & \bullet & \bullet \\ \bullet & \bullet & \bullet \end{bmatrix} \begin{bmatrix} 0 & G_i^T & (\bar{A}_{ii} - (1 + \Delta q_k) L_i \bar{C}_i)^T P_i \\ 0 & 0 & 0 \\ 0 & 0 & \bar{C}_i^T L_i^T P_i \\ -\gamma^2 I_i & 0 & \bar{B}_i^T P_i \\ \bullet & -I_i & 0 \\ \bullet & \bullet & -P_i \end{bmatrix} < 0.$$

By setting $X_i = P_i^{-1}, Y_i = L_i \bar{C}_i X$ and applying the congruent transformation: $T_i = \text{blkdiag}\big(X_i,\, X_i,\, X_i,\, I_i,\, I_i,\, X_i\big)$, it follows directly that $\hat{\Xi}_j = T_i \Xi_j T_i$ in accordance with (40). Hence, the proof is concluded.

Remark 6. *The proposed method demonstrates satisfactory performance and effectiveness. However, it requires solving Linear Matrix Inequalities (LMIs), which may introduce a non-negligible computational burden. As a result, the associated complexity could limit its applicability in real-time implementations. Nevertheless, the proposed methodology is well-suited for offline applications, as demonstrated by the presented simulation results.*

5. Simulation results and discussion

This section validates the performance of the developed distributed observer, enhanced with RBF–NN fault estimation and AGC/ACE-based regulationin a three-area microgrid. Four scenarios of increasing difficulty are considered: (i) nominal operation; (ii) communication effects without faults; (iii) actuator faults only; and (iv) the worst-case combination of delays, quantization, and faults. The simulation results indicate the robustness and adaptability of the developed scheme across operating conditions, with bounded states and recovery of performance metrics following disturbances. All simulations run with sampling period $T_s = 0.02\,\text{second}$ (50 Hz). Unless otherwise stated, the ACE loop is enabled and the tie-line schedule is feasible and balanced, maintaining physical realizability.

Each area $i \in \{1, 2, 3\}$ is represented by the linearized power module, turbine-governor, and tie-line dynamics; the composite continuous-time system is discretized through zero-order hold. The observed output is $y_i = [\Delta\omega_i \;\; \Delta P_{\text{tie},i}]^\top$. The control law is designed as in section 3.2, and the state estimate $\hat{\mathcal{X}}_{ip}$ is computed by the proposed observer **Equation 23** with gain L_i obtained by solving the LMI in theorem 2 using YALIMP toolbox, with MOSEK solver. Actuator faults enter additively at the input channel.

Figure 2 illustrates the nominal performance of the system in the absence of actuator faults and time-varying delays, demonstrating stable dynamics and state dynamics that remain well damped with tightly regulated frequency and tie line power. From **Figure 3**, estimation errors decay rapidly and control inputs stay within moderate bounds. Thus, the system's response remains dynamic within its design limits, reflecting effective coordination across interconnected areas.

Figure 4 shows that the random time delays induce a small phase offset and mild overshoot,

extending the settling time relative to the nominal case in **Figure 2**. The closed loop remains stable; frequency excursions are suppressed, and tie-line power errors stay within design tolerances, as confirmed by the estimation-error norms and applied control inputs in **Figure 5**. The corresponding output reconstruction is illustrated in **Figure 6**, where the true, post-network measured, and observer-estimated trajectories of $\Delta\omega$ and ΔP_{tie} are overlaid for all three areas; the close agreement between the true and estimated signals verifies that the observer recovers the regulated outputs despite quantization and time-varying delays. A complementary view of the full state trajectories under the same delay condition is provided in **Figure 7**, confirming uniformly bounded $\Delta\omega$, ΔP_{mech}, ΔP_{vi}, and ΔP_{tie} across the three areas.

Building on this baseline, **Figure 8** demonstrates the combined effect of actuator faults and random time delays. Frequency and tie-line power show larger oscillations and the slowest settling among the three cases; nevertheless, the controller retains bounded states and eventual recovery. Even in this worst-case scenario, the designed observer-based controller succeeds in restoring stability. The associated post-network output signals under this combined time-delay and faulty-actuator condition are presented in **Figure 9**, where the observer estimates continue to track the true outputs of $\Delta\omega$ and ΔP_{tie} with bounded residuals, confirming the fault-isolation capability of the RBF-NN augmentation.

In **Figure 10**, we compare the quantized H_∞ filtering [13] and the proposed H_∞-based RBF-NN scheme under the worst-case scenario of simultaneous actuator faults, time-varying delays, and quantization. The proposed scheme reduces $|\Delta\omega|$ by $\sim 33\%$ from ~ 0.48 to 0.32, $|\Delta P_{\text{tie}}|$ by $\sim 50\%$ from 0.38 to 0.19, and $|\Delta P_{\text{mech}}|$ by $\sim 27\%$ from 0.45 to 0.33 from the peak responses.

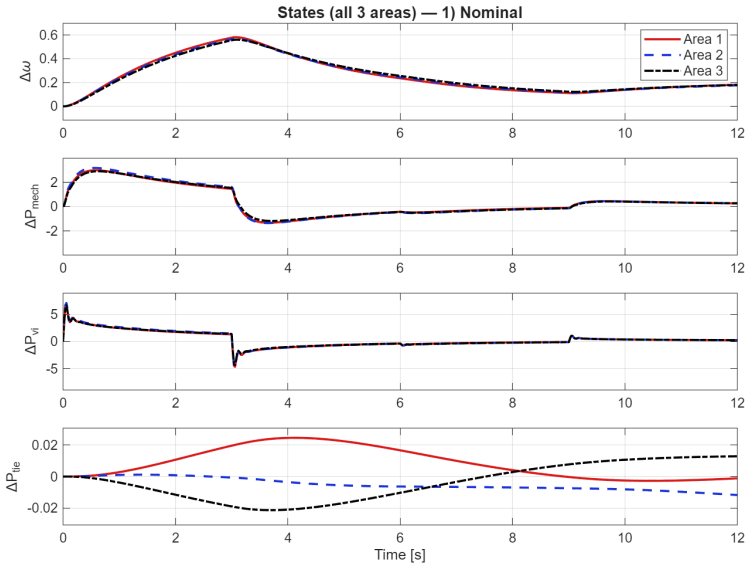


Figure 2. States over time for the nominal scenario (all three areas)

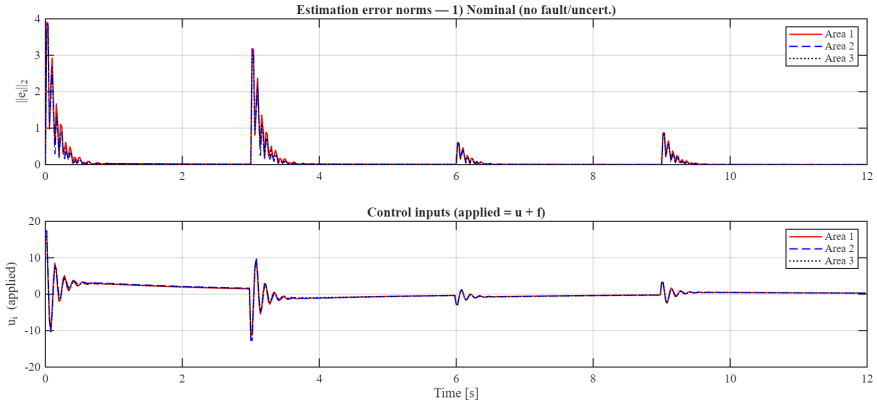


Figure 3. Estimation error norms (top) and applied control inputs (bottom)

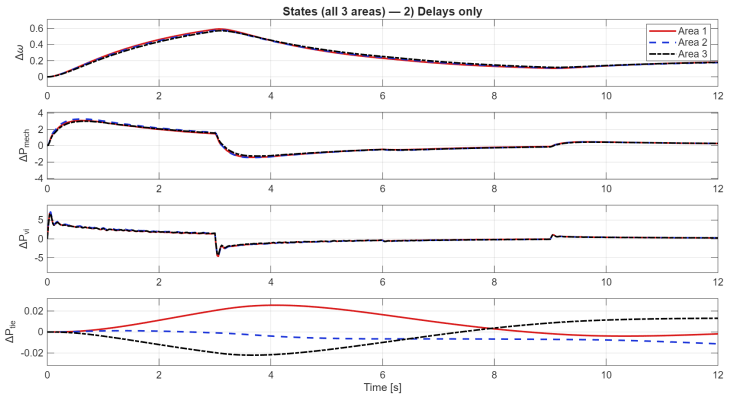


Figure 4. States trajectories under time-delay impact

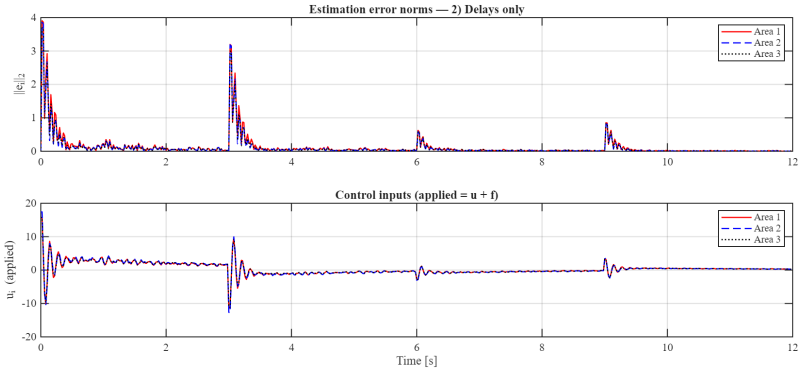


Figure 5. Estimation Error and Control signal in the face of time delay

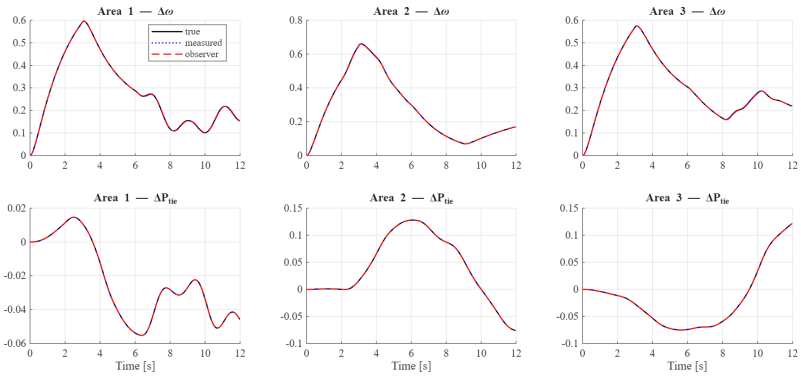


Figure 6. Outputs: true, measured (post-network), and observer estimates for $\Delta\omega$ and ΔP_{tie}

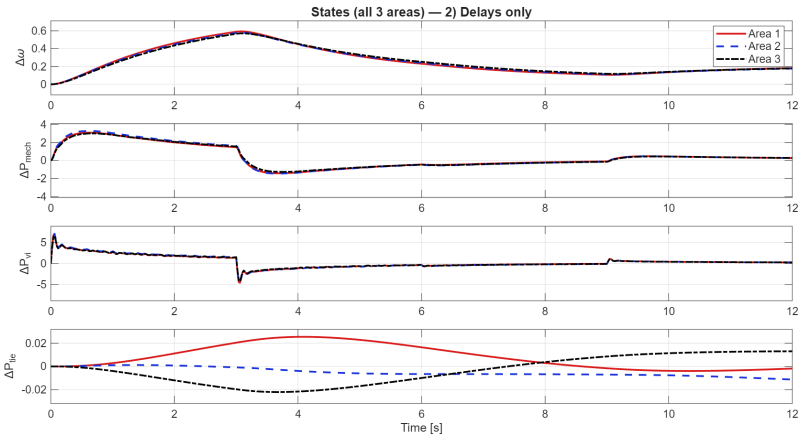


Figure 7. States of a multi-power system subject to time delay

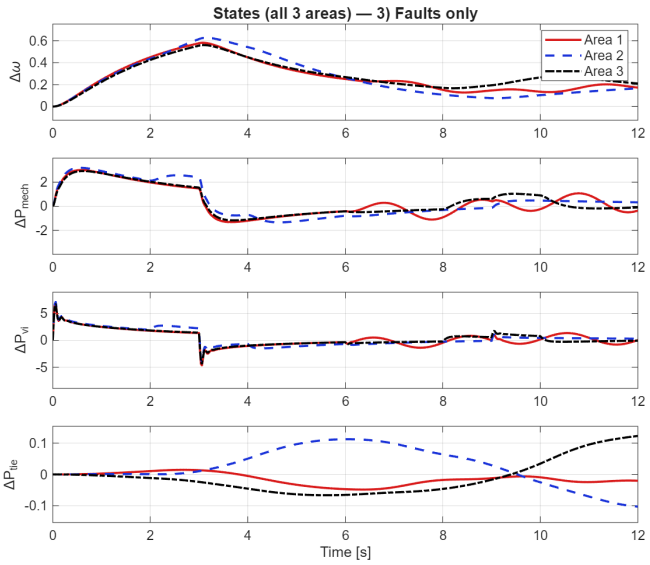


Figure 8. States of multi-area power subjected to actuator fault

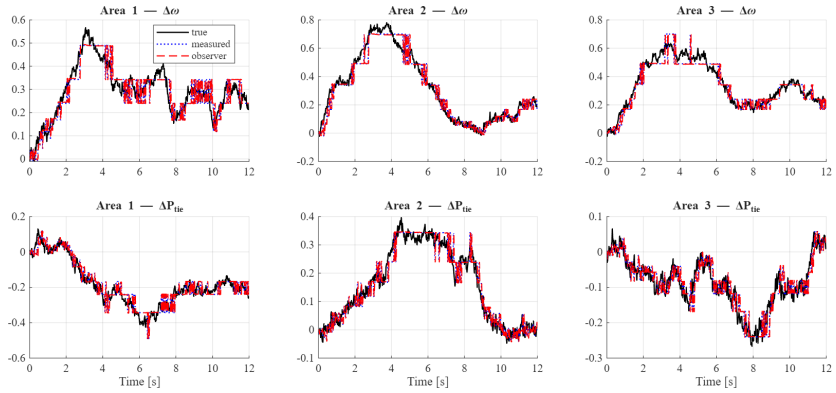


Figure 9. Output signals of the multi-area subject to time-delay and faulty signal

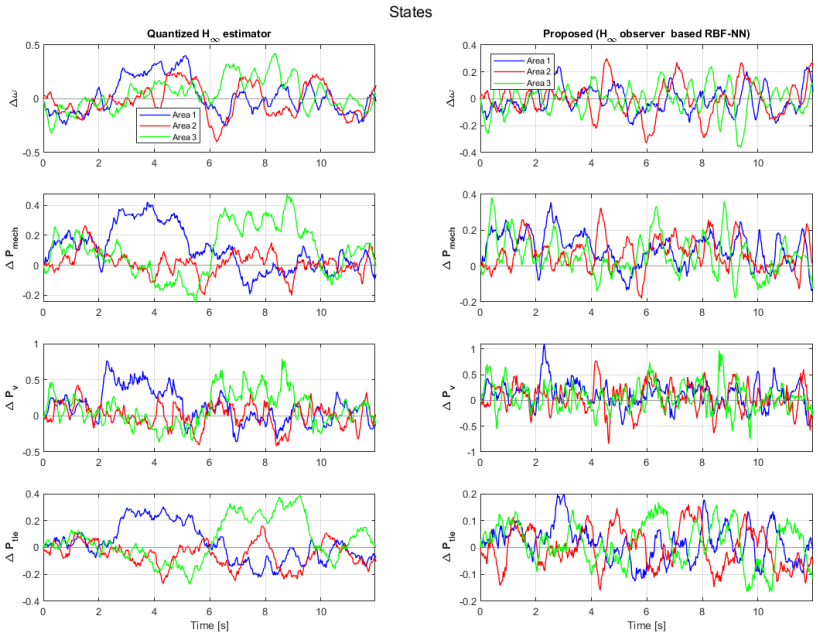


Figure 10. State-response comparison of the quantized H_∞ filter[13] and the proposed scheme under actuator faults, time-varying delays, and quantization

The improvement does not arise solely from stronger attenuation. The embedded RBF-NN structure adapts to fault-induced uncertainties during operation, allowing the observer to compensate for variations introduced by degraded actuators and delayed measurements. This adaptive behavior, combined with the disturbance-rejection capability of the distributed H_∞ framework, maintains bounded trajectories across all interconnected areas even under severe network-induced constraints.

6. Conclusions

This paper presented a distributed observer scheme for the simultaneous estimation of system states and actuator faults in multi-area interconnected power systems subject to actuator faults, time-varying delays, quantization, and external disturbances. The developed augmented observer incorporates fault dynamics into the estimation process, while an RBF-NN with a projection-based adaptive law is employed to approximate unknown actuator-fault effects and maintain bounded adaptive estimates. Sufficient LMI-based conditions are derived to ensure the stability of the distributed observer-error dynamics and a prescribed ℓ_2-gain performance level with respect to the lumped exogenous input, using a delay-dependent Lyapunov-Krasovskii functional with free-weighting matrices.

Compared with existing observer-based approaches, the proposed framework offers improved adaptability to networked multi-area systems by explicitly accounting for communication-induced delays and quantization effects. The numerical results obtained from the three-area benchmark system, summarized in **Figure 10**, demonstrate the practical effectiveness of the proposed scheme. Under simultaneous actuator faults, time-varying delays, and quantization, the peak deviations of the regulated frequency and tie-line power are reduced by approximately 33% for $|\Delta\omega|$ and 50% for $|\Delta P_{\text{tie}}|$, together with a 27% reduction in $|\Delta P_{\text{mech}}|$, compared with a quantized H_∞ baseline observer. These results indicate that the proposed observer confines disturbance effects primarily within the actuator-side state, thereby reducing their influence on the regulated frequency and tie-line power outputs.

In summary, the proposed observer offers a robust estimation framework for networked power systems with actuator faults, communication delays, quantization and external disturbances. Future work will focus on several practical extensions, including more severe cyber attack scenarios and wireless network control.

Acknowledgments

None.

Funding

None.

Conflict of interest

The authors have no relevant financial or non-financial interests to disclose.

Author contributions

Conceptualization: Nezar M. Alyazidi, Mutaz M. Hamdan
Formal analysis: Nezar M. Alyazidi
Investigation: Nezar M. Alyazidi, Mutaz M. Hamdan
Methodology: Nezar M. Alyazidi, Mutaz M. Hamdan, Ahmed Eltayeb, Mahmoud S. AbouOmar
Software: Nezar M. Alyazidi, Gamil Ahmed
Writing–original draft: Nezar M. Alyazidi, Mutaz M. Hamdan
Writing–review & editing: All authors.

Availability of data

The datasets and code generated or analyzed during the current study are available from the corresponding author on reasonable request.

AI tools statement

All authors confirm that no AI tools were used in the preparation of this manuscript.

References

1. Benosman M. A survey of some recent results on nonlinear fault tolerant control. *Math Probl Eng.* 2010;2010(1):586169. https://doi.org/10.1155/2010/586169
2. Tran HM, Trinh H. Distributed functional observer based fault detection for interconnected time-delay systems. *IEEE Syst J.* 2017;13(1):940-951. https://doi.org/10.1109/JSYST.2017.2759257
3. Zhang ZH. Interval observer-based fault isolation for discrete-time fuzzy interconnected systems with unknown interconnections. *IEEE Trans Cybern.* 2017;47(9):2413-2424. https://doi.org/10.1109/TCYB.2017.2707462
4. Zhang K, Jiang B, Shi P. Distributed fault estimation observer design with adjustable parameters for a class of nonlinear interconnected systems. *IEEE Trans Cybern.* 2018;49(12):4219-4228. https://doi.org/10.1109/TCYB.2018.2860588
5. Yang H, Huang C, Jiang B, Polycarpou MM. Fault estimation and accommodation of interconnected systems: A separation principle. *IEEE Trans Cybern.* 2018;49(12):4103-4116. https://doi.org/10.1109/TCYB.2018.2857820

6. Xia J, Jiang B, Zhang K. Unknown input observer-based distributed fault estimation of discrete-time nonlinear interconnected systems. *Int J Control Autom Syst.* 2022;20(3):803-812. https://doi.org/10.1007/s12555-021-0082-4
7. Song X, Man J, Song S, Ahn CK. Finite-time fault estimation and tolerant control for nonlinear interconnected distributed parameter systems with Markovian switching channels. *IEEE Trans Circuits Syst I Regul Pap.* 2021;69(3):1347-1359. https://doi.org/10.1109/TCSI.2021.3129372
8. Mahmoud MS, Memon AM, Shi P. Observer-based fault-tolerant control for a class of nonlinear networked control systems. *Int J Control.* 2014;87(8):1707-1715. https://doi.org/10.1016/j.jfranklin.2010.01.007
9. Mao Z, Jiang B, Shi P. Observer-based fault-tolerant control for a class of nonlinear networked control systems. *J Franklin Inst.* 2010;347(6):940-956. https://doi.org/10.1016/j.jfranklin.2010.01.007
10. Alanis AY, Alvarez JG, Sanchez OD, Hernandez HM, Valdivia-G A. Fault-tolerant closed-loop controller using online fault detection by neural networks. *Machines.* 2024;12(12):844. https://doi.org/10.3390/machines12120844
11. Stiefelmaier J, Böhm M, Sawodny O, Tarín C. Parity space-based fault diagnosis in piecewise linear systems. *IFAC-PapersOnLine.* 2023;56(2):10868-10873. https://doi.org/10.1016/j.ifacol.2023.10.764
12. Benjemaa R, Khorchani N, Elhsoumi A, Abdelkrim MN. Fault detection based on the parity space approach for neutral time delay systems. In: *Proceedings of the 2025 IEEE 22nd International Multi-Conference on Systems, Signals & Devices (SSD).* IEEE; 2025:1-5. https://doi.org/10.1109/SSD64182.2025.10989971
13. Mahmoud MS, Alyazidi NM. Quantized H_∞ estimator over communication networks for distributed generation units. *IEEE Trans Syst Man Cybern Syst.* 2017;50(3):1134-1146. https://doi.org/10.1109/TSMC.2017.2734167
14. Alyazidi NM, Al-Wajih YA, Mahmoud MS. Iterative learning control for load frequency in cyber-attacked multi-area power systems. *IEEE Access.* 2023;11:95481-95492. https://doi.org/10.1109/ACCESS.2023.3309150
15. Thanh TV, Le CQ, Viet DT, Hieu NH, Le VD. Advanced frequency control strategy for power systems with high renewable energy penetration: A battery energy storage system approach. *Int J Optim Control Theor Appl.* 2025;15(4):625. https://doi.org/10.36922/IJOCTA025150076
16. Ouzaz M, El Assoudi A, Soulami J, El Yaagoubi EH. Simultaneous state and fault estimation for Takagi-Sugeno implicit models with Lipschitz constraints. *Int J Optim Control Theor Appl.* 2021;11(1):100-108. https://doi.org/10.11121/ijocta.01.2021.00877
17. Li X, Qin H, Han H, Wu X. Fault diagnosis and fault-tolerant control design for nonlinear networked systems: An interval type-2 TS fuzzy approach. *IEEE Trans Autom Sci Eng.* 2026. https://doi.org/10.1109/TASE.2026.3656456
18. Qiao MY, Chang XH, Park JH. Observer-based fault estimation and compensation control for nonlinear multi-delays systems with multi-source faults. *IEEE Trans Autom Sci Eng.* 2026;23:7587-7598. https://doi.org/10.1109/TASE.2026.3678544
19. Wu X, Li N, Zhang T, Ding D. Fault detection based on time-delay dependent H_-/H_∞ observers for linear discrete systems. *IEEE Access.* 2026. https://doi.org/10.1109/ACCESS.2026.3661489
20. Wu J, Geng Y, Wang J. Robust H_∞ fault-tolerant control with mixed time-varying delays. *Actuators.* 2026;15(2):73. https://doi.org/10.3390/act15020073
21. Wang B, Wang Y, Zhang Z, Tang M, Vakil G, Yang T. Review of fault-tolerant permanent magnet synchronous machine design and control for future aircraft application. *Chin J Electr Eng.* 2025;11(2):165-187. https://doi.org/10.23919/CJEE.2025.000139
22. Jia F, Cao F, He X. Active fault-tolerant control against intermittent faults for state-constrained nonlinear systems. *IEEE Trans Syst Man Cybern Syst.* 2024;54(4):2389-2401. https://doi.org/10.1109/TSMC.2023.3344292
23. Chen P, Yu L, Zhang D. Event-triggered sliding mode control of power systems with communication delay and sensor faults. *IEEE Trans Circuits Syst I Regul Pap.* 2020;68(2):797-807. https://doi.org/10.1109/TCSI.2020.3035603.
24. Wang H, Li J, He C, Song C. Robust adaptive optimal fault-tolerant control scheme for multi-machine power systems via the stabilizing two-stage policy iteration framework. *IEEE Trans Circuits Syst I Regul Pap.* 2025. https://doi.org/10.1109/TASE.2025.3603734
25. Huang S, Xiong L, Zhou Y, Gao F, Jia Q, Li X, Li X, Wang Z, Khan MW. Robust distributed fixed-time fault-tolerant control for shipboard microgrids with actuator fault. *IEEE Trans Transp Electrif.* 2024;11(1):1791-1804. https://doi.org/10.1109/TTE.2024.3411289
26. Grande D, Peruffo A, Salavasidis G, Anderlini E, Fenucci D, Phillips AB, Kosmatopoulos EB, Thomas G. Passive fault-tolerant augmented neural Lyapunov control: A method to synthesise control functions for marine vehicles affected by actuators faults. *Control Eng Pract.* 2024;148:105935. https://doi.org/10.1016/j.conengprac.2024.105935
27. Saif AWA, Wang X, Yang F. New results on the observer-based H_∞ control for uncertain nonlinear networked control systems with random packet losses. *IEEE Access.* 2019;7. https://doi.org/10.1109/ACCESS.2019.2900551

28. Liu Z, Li Y, Li L, Ma K, Yang Y. On the security and stability for wireless networked control systems with external attack and disturbances. *Int J Robust Nonlinear Control*. 2022. https://doi.org/10.1002/rnc.6260
29. Xu Z, Yang X, Li X, Lu J. Input-to-state stability of switched network control systems under unknown deception attacks. *IEEE Trans Autom Sci En*. 2024. https://doi.org/10.1109/TCYB.2024.3376695
30. Lin H, Dong J, Park JH. Observer-based H_∞ fault-tolerant tracking control of multi-agent systems with nonideal communication links and external disturbances. *IEEE Trans Autom Sci Eng*. 2025;22:14096-14107. https://doi.org/10.1109/TASE.2025.3557951
31. Peng C, Yue D, Tian E, Gu Z. Observer-based fault detection for networked control systems with network quality of services. *Appl Math Model*. 2010;34:1653-1661. https://doi.org/10.1016/j.apm.2009.09.014
32. Mu Y, Zhang H, Yan Y, Xie X. Distributed observer-based robust fault estimation design for discrete-time interconnected systems with disturbances. *IEEE Trans Cybern*. 2023. https://doi.org/10.1109/TCYB.2022.3232531
33. Deng C, Wen C. Distributed resilient observer-based fault-tolerant control for heterogeneous multiagent systems under actuator faults and DoS attacks. *IEEE Trans Control Netw Syst*. 2020;7(3):1308-1318. https://doi.org/10.1109/TCNS.2020.2972601
34. Huang S, Ren J, Ma Z, Peng C, Su H. Distributed observer-based H_∞ fault-tolerant control for DC microgrids with sensor fault. *IEEE Trans Circuits Syst I Regul Pap*. 2021;68(4):1659-1669. https://doi.org/10.1109/TCSI.2020.3048971
35. Sun HT, Chen X, Zhang Z, Ge X, Peng C. Data-driven event-triggered sliding mode secure control for autonomous vehicles under actuator attacks. *IEEE Trans Cybern*. 2024. https://doi.org/10.1109/TCYB.2024.3490656
36. Mu Y, Zhang H, Xi R, Gao Z. State and fault estimations for discrete-time TS fuzzy systems with sensor and actuator faults. *IEEE Trans Circuits Syst II Express Briefs*. 2021;68(10):3326-3330. https://doi.org/10.1109/TCSII.2021.3067708
37. Alyazidi NM, Mahmoud MS. $\mathcal{L}_1$ adaptive networked controller for islanded distributed generation systems in a microgrid. *Int J Syst Sci*. 2018;49(12):2507-2524. https://doi.org/10.1080/00207721.2018.1487093
38. Mahmoud MS. Estimator design for networked control systems with nonstationary packet dropouts. *IMA J Math Control Inf*. 2013;30(3):395-405. https://doi.org/10.1093/imamci/dns030

Nezar M. Alyazidi *received the B.Sc. degree from Hadramout University of Science and Technology (HUST), Hadramout, Yemen, in 2006, and the M.Sc. and Ph.D. degrees in systems and control engineering from King Fahd University of Petroleum and Minerals (KFUPM), Dhahran, Saudi Arabia, in 2012 and 2017, respectively. He served as a Lecturer-B with the Systems Engineering Department, KFUPM, from 2013 to 2017, and as a Postdoctoral Fellow in the same department from 2017 to 2018. He is currently an Associate Professor with the Department of Control and Instrumentation Engineering, KFUPM. He is also a Research Scholar Fellow with the Interdisciplinary Research Center for Smart Mobility and Logistics, KFUPM. His research interests include nonlinear control, adaptive control, reinforcement learning, optimization algorithms, distributed renewable generation systems, time-delay systems, networked control systems, and secure control systems.*
https://orcid.org/0000-0001-8977-9302.

Mutaz M. Hamdan *is an Assistant Professor in the Faculty of Engineering at Al-Ahliyya Amman University, Jordan, where he has been serving since 2023. He earned his B.Sc. degree from Palestine Polytechnic University, Hebron, Palestine, in 2006. He received his M.Sc. and Ph.D. degrees in Systems and Control Engineering in 2012 and 2019, respectively, from the Systems Engineering Department at King Fahd University for Petroleum and Minerals (KFUPM), Dhahran, Saudi Arabia. Dr. Hamdan completed a Postdoctoral Fellowship with the Systems Engineering Department at KFUPM (2020–2021). He subsequently served as an Assistant Professor in the Mechanical Engineering Department at the National University College of Technology, Amman, Jordan (2022–2023). His research interests include secure control of cyber-physical systems, distributed control systems, and intelligent control systems. Dr. Hamdan has over ten years of academic and research experience. He has co-authored a book published by Elsevier, authored more than 19 peer-reviewed journal articles, and holds three U.S. patents. He also serves as a reviewer for several high-impact journals in the field of systems and control engineering.*
https://orcid.org/0000-0002-4516-571X.

Ahmed Eltayeb *received his Ph.D. in Electrical Engineering (Control and Mechatronics) from Universiti Teknologi Malaysia. He is currently a researcher at the Interdisciplinary Research Center for Smart Mobility and Logistics and a lecturer in the Department of Control and Instrumentation Engineering at King Fahd University of Petroleum and Minerals (KFUPM), Saudi Arabia. His research interests include adaptive and intelligent control systems, unmanned aerial vehicles (UAVs), robotics, multi-agent systems, and advanced optimization techniques.*
https://orcid.org/0000-0002-9151-4116.

Mahmoud S. AbouOmar *received the B.Sc. degree in Electronics Engineering and the M.Sc. degree in Industrial Electronics and Control Engineering from the Faculty of Electronic Engineering, Menoufia University, Egypt. He received the Ph.D. degree in Traffic*

Information Engineering and Control, with a specialization in Automatic Control and Intelligent Systems, from the School of Automation, Wuhan University of Technology, China, in 2021. He is currently a Postdoctoral Fellow at the Interdisciplinary Research Center for Smart Mobility and Logistics (IRC-SML), King Fahd University of Petroleum & Minerals (KFUPM), Dhahran, Saudi Arabia. His research interests include artificial intelligence, optimization techniques, system identification and control, with applications in energy systems, mechatronics, new energy vehicles, and intelligent transportation systems.
https://orcid.org/0000-0001-5370-4683.

Gamil Ahmed *received the B.Sc. In Computer Engineering from Al Mosul University, Al Mosul, Iraq, in 2005. From 2007 to 2013, he served as a lecturer assistant in the Electrical and Computer Department, Communication and Computer Engineering, at Ibb University, Ibb, Yemen. He obtained his M.S. degree from King Fahd University of Petroleum and Minerals (KFUPM), Dhahran, Saudi Arabia, in 2017. He received his Ph.D. in Computer Engineering from the Computer Engineering Department at King Fahd University of Petroleum and Minerals (KFUPM) in Dhahran, Saudi Arabia, in 2022. He is currently a postdoc fellow in the Smart Mobility and Logistics Center at King Fahd University of Petroleum and Minerals (KFUPM), Dhahran, Kingdom of Saudi Arabia. His research interests include Machine Learning, Intelligent Transportation Systems (ITS), Smart Cities, the Internet of Things (IoT), Multi-Agent Systems, IoD, and wireless sensor networks (WSN).*
https://orcid.org/0000-0002-1411-264X.

Maged S. Al-Quraishi *is a biomedical engineer specializing in neuro-engineering, biomedical signal processing, machine learning, and bio-robotics. After earning his PhD, he pursued postdoctoral research at UTP, where he expanded his work on translational neurotechnology and contributed to high-impact, cutting-edge research initiatives. He is currently a postdoctoral fellow at King Fahd University of Petroleum and Minerals (KFUPM), leading innovative projects that bridge engineering and medicine to address critical challenges in neurological health and human–machine interaction. His research agenda emphasizes interdisciplinary collaboration at the interface of engineering and medicine, with the goal of advancing quantitative methods and translational technologies in neuroscience and healthcare.*
https://orcid.org/0000-0003-0911-789X.

An International Journal of Optimization and Control: Theories & Applications (https://accscience.com/journal/ijocta)

This work is licensed under a Creative Commons Attribution 4.0 International License. The authors retain ownership of the copyright for their article, but they allow anyone to download, reuse, reprint, modify, distribute, and/or copy articles in IJOCTA, so long as the original authors and source are credited. To see the complete license contents, please visit http://creativecommons.org/licenses/by/4.0/.